MATERIALS CHEMISTRY
FRONTIERS

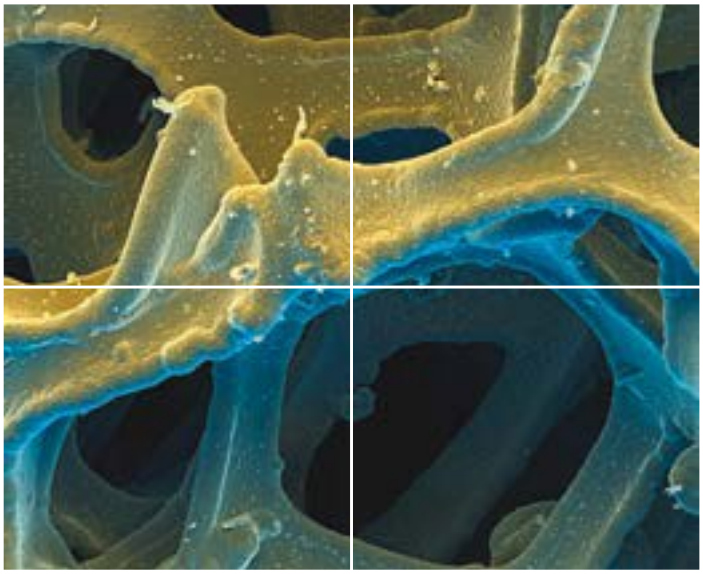

Accepted Manuscript

This article can be cited before page numbers have been issued, to do this please use: I. B. Dogru, C. Kosak Soz, D. A. Press, R. Melikov, E. Begar, D. Conkar, E. N. Firat Karalar, E. Yilgor, I. Yilgör and S. Nizamoglu, *Mater. Chem. Front.*, 2017, DOI: 10.1039/C7QM00281E.

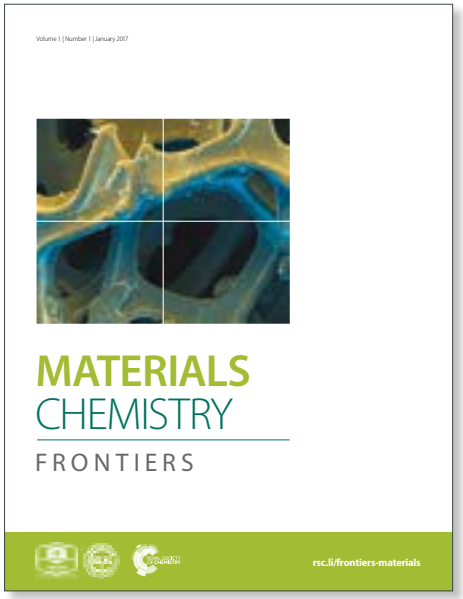

View Article Online
DOI: 10.1039/C7QM00281E

Materials Chemistry Frontiers

ARTICLE

3D Coffee Stain

Itir Bakis Dogru[1], Cagla Kosak Soz[2,5], Daniel Aaron Press[3], Rustamzhon Melikov[3], Efe Begar[4], Deniz Conkar[4], Elif Nur Fırat Karalar[4], Emel Yilgor[2,5], Iskender Yilgor[1,2,5] and Sedat Nizamoglu[1,3,5,*]

Received 00th January 20xx,
Accepted 00th January 20xx

DOI: 10.1039/x0xx00000x

www.rsc.org/

When a liquid droplet (e.g., coffee, wine, etc.) is splattered on a surface, the droplet dries in a ring-shaped stain (1). This widely observed pattern in everyday life occurs due to the phenomenon which is known as coffee stain (or coffee ring) effect (2). While the droplet dries, the capillary flow moves and deposits the particles toward the pinned edges, which shows a 2D ring-like structure (3, 4). Here we demonstrate the transition from a 2D to a 3D coffee stain that has a well-defined and hollow sphere-like structure, when the substrate surface is switched from hydrophilic to superhydrophobic. The 3D stain formation starts with the evaporation of the pinned aqueous colloidal droplet placed on a superhydrophobic surface that facilitates the particle flow towards liquid-air interface. This leads to a spherical skin formation and a cavity in the droplet. Afterwards the water loss in the cavity due to pervaporation leads to a bubble nucleation and growth, until complete evaporation of the solvent. In addition to the superhydrophobicity of the surface, the concentration of solution also has a significant effect on 3D coffee stain formation. Advantageously 3D coffee stain formation in pendant droplet configuration enables the construction of all-protein lasers by integrating silk fibroin with fluorescent proteins. No tools, components and/or human intervention are needed after the construction process is initiated, therefore, 3D coffee-stain holds promise for building self-assembled and functional 3D constructs and devices from colloidal solutions.

Introduction

Self-assembly is a spontaneous process that forms patterns or structures by using molecular scale movements and interactions (5, 6). This process with non-covalent interactions enables the extension of the structures to visible length scales (7). A simple way to achieve self-assembled structures at macroscale is the deposition of a colloidal solution onto a substrate, in which the interface between the substrate and solution controls the patterns of the colloids after evaporation. However, formation of free-standing and functional 2D and 3D structures generally requires the use of complex fabrication techniques, such as; photolithography (8), microcontact-printing (9), inkjet-printing (10), milling (11), laser microfabrication (12) at all scales. Even though there are non-complex techniques to generate patterns with self-assembly techniques, these structures have short spatial extents and building a macroscale structure in regular 3D pattern with embedded functionality are limited (13-18).

[1]Graduate School of Biomedical Sciences and Engineering, [2]Department of Chemistry, [3]Department of Electrical and Electronics Engineering, [4]Department of Molecular Biology and Genetics, [5]KUYTAM Surface Science and Technology Research Center
Koc University, Sariyer, Istanbul, 34450 Turkey
*Email: snizamoglu@ku.edu.tr

Electronic Supplementary Information (ESI) available: [details of any supplementary information available should be included here]. See DOI: 10.1039/x0xx00000x

Coffee stain effect that uses the evaporation of droplets containing colloidal suspensions and solutions on a surface is a simple technique to generate 2D self-assembled structures on large dimensions (19, 20). In an evaporating drop, a capillary flow is generated to replenish the liquid that is lost at the edges (21). This flow drags particles towards the three phase (air-liquid-solid) contact line, forming the classical 2D ring-shaped stain in particle suspensions (21-23). So far coffee stain effect has been used as a simple, autonomous and time-efficient approach for 2D pattern formation (21, 24, 25). Furthermore, a large variety of morphologies can be obtained via surface-liquid-air interactions (26-35). Different from previous reports, here we demonstrate the connection, control and transition of coffee stains from 2D to 3D structures under the same conditions including time, concentration, temperature and solution pinning. While hydrophilic surfaces with water contact angles smaller than 90° (WCA < 90°) shows the formation of 2D coffee stains, superhydrophobic surfaces (WCA > 150°) leads to the formation of 3D spherical structures, which we term as the “3D coffee stain”. Furthermore, we also investigate the evaporation of pendant aqueous colloidal droplets, which result in the formation of high-quality silk fibroin spheres that incorporate fluorescent proteins for all-protein lasers.

What is a 3D coffee stain and how does it form?

DOI: 10.1039/C7QM00281F

The coffee stain effect, which forms the classical 2D structure, can be used to generate self-supporting 3D structures. To investigate the 3D coffee stain formation, an aqueous photoluminescent silk fibroin solution modified with enhanced green fluorescent protein (eGFP) is placed on a superhydrophobic surface, with a WCA greater than 150° (36). While the same protein solution generates a 2D ring on a hydrophilic surface (Fig. 1a), a superhydrophobic surface allows the formation of a 3D spherical structure (Fig. 1b). The process from liquid droplet to 3D solid form can be divided into two main stages. As shown in Fig. 1b, in the first stage (0 - 16 min) the droplet volume becomes smaller due to evaporation. The spherical droplets exhibit d-square law behavior ($\boldsymbol{D^2/D_0^2 = 1 - kt/D_0^2}$) (Fig. 1c), where ($D$) is the droplet diameter as a function of time during the evaporation process, (D_0) is the initial droplet diameter, (k) is the evaporation rate and (t) is the time. This square law behavior means that the solvent and air interface dominates the droplet vaporization (37). The diameter of the droplet decreases (k = 0.037 mm^2/s) to a steady-state value and then stays approximately the same (Fig. 1c). In addition, it is important to note that the pinned contact area both in 2D and 3D stain formation (Fig. 1a and 1b, respectively) stays constant during evaporation. To keep the contact area fixed, the particles in the liquid flow in a radial motion towards the edges as in the 2D coffee stain formation (2). As a result, the formation of 3D coffee stain is preceeded with the construction of the 2D ring at the three phase contact line, which can be considered as the first stage.

While the evaporation continues, the solvent permeation flux is higher on the surface of the droplet than its interior and the flow due to the radial migration piles up the colloidal particles on the

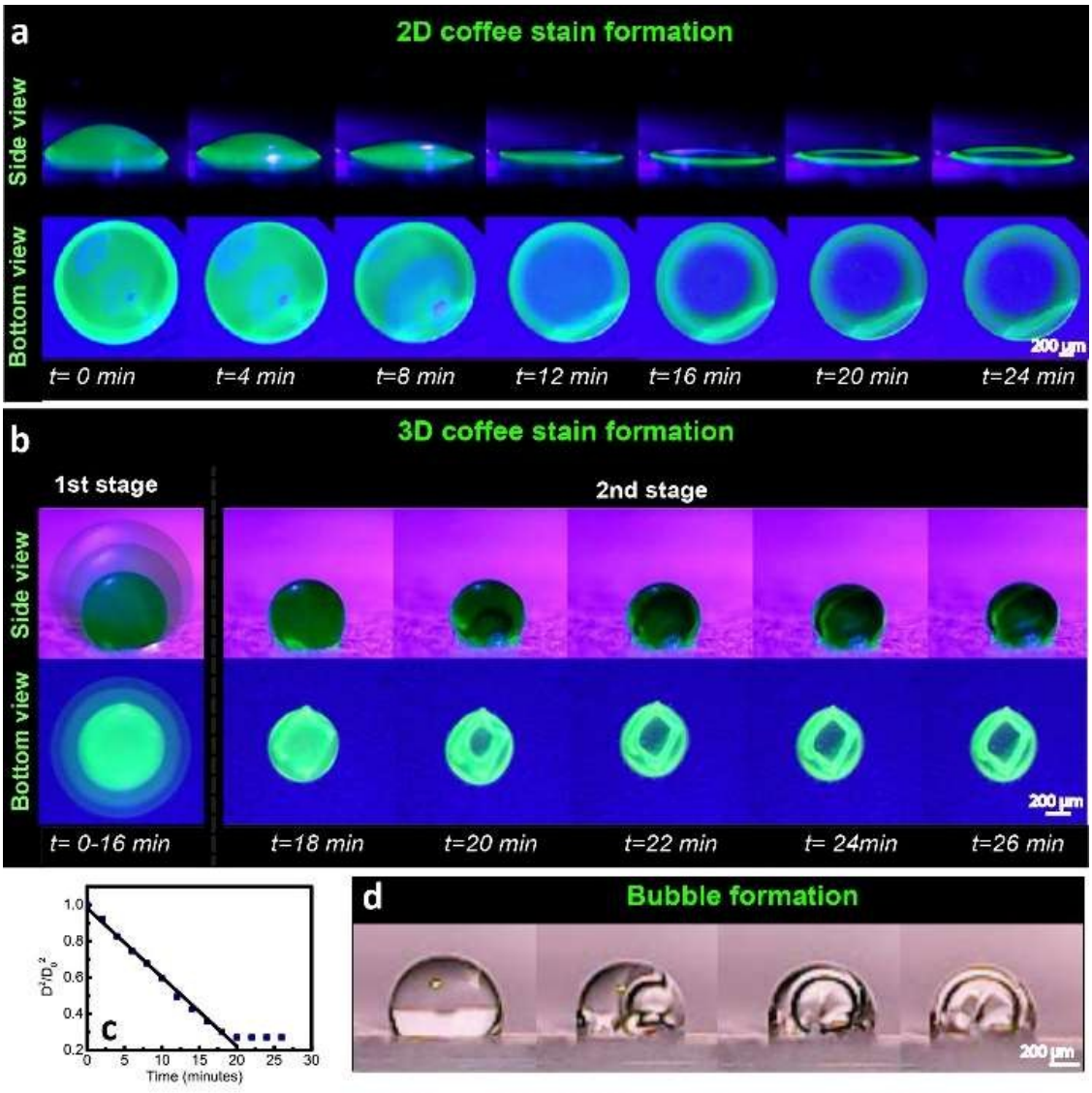

Fig. 1 Formation of **(a)** 2D and **(b)** 3D coffee stains from a colloidal, aqueous eGFP modified silk fibroin droplet placed on a hydrophilic poly(methyl methacrylate) (PMMA) (1a) and a superhydrophobic polydimethylsiloxane-urea (SHPSU) surface (1b) with water contact angles of 64° and 165°, respectively. **(c)** The change in the droplet diameter (D^2/D_0^2) on the superhydrophobic surface as a function of time. **(d)** Demonstration of bubble formation using transparent silk fibroin solution on the superhydrophobic surface.

DOI: 10.1039/C7QM00281E

edges of the 2D coffee stain. The continued stacking of the particles initiates the formation of droplet skin on the initial coffee stain ring. Furthermore, since the surface energy of water (72.6 mN/mm) is much higher than that of silk fibroin (43-52 mN/mm) (38), skin formation also leads to substantial reduction in the overall surface energy of the system and thus, it is thermodynamically favorable. Formation of the 3D skin becomes completed on top of the 2D ring at the end of the first stage.

In the second stage (18 - 26 min) the radius of the skin does not significantly change (Fig. 1b) while evaporation continues. This is due to the formation of a water vapor permeable, semi-crystalline and robust silk fibroin skin on the outer layer of the droplet (Fig. S1). At this point the droplet has a fairly dense solid-air interface, while the inside is filled with liquid. As the evaporation continues a bubble nucleates in the 3D skin (Fig. 1b), which is more clearly observable for a transparent silk fibroin droplet (Fig. 1d). The volume of the silk fibroin solution decreases as the solvent permeates through the skin, which results in the expansion of the bubble inside the droplet and reinforcement of the 3D skin. The 3D spheroid surfaces remain fairly smooth during the evaporation process (as provided in Video S1 in Supplementary Information). At the end of the evaporation, 3D coffee stain is formed. The structure

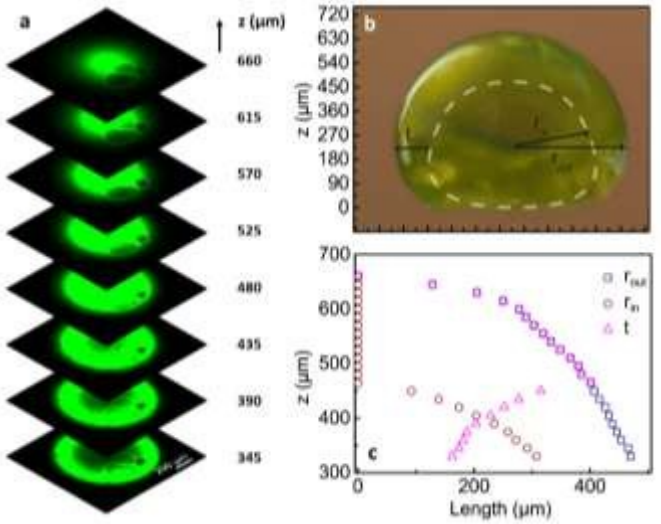

Fig. 2 (a) Confocal z-stack images of eGFP modified silk fibroin 3D coffee stain formed on the superhydrophobic surface, **(b)** the side view and schematic description of the 3D stain with outer (r_{out}) and inner (r_{in}) radius, and wall thickness (t) in the xy plane, and **(c)** their values in z-direction.

of a 3D coffee stain was analyzed by using confocal microscopy (Fig. 2a). The 3D coffee stain has sub-millimeter dimensions with a height of 660 μm (in z-direction) and a maximum outer radius ($\mathbf{r_{out}}$) of 477 μm (in the xy plane) (Fig. 2b and 2c). Starting from the top (z=660 μm) while we image the sphere downwards (-$\hat{\boldsymbol{z}}$ direction), we observe the first cavity at z=465 μm plane. At this point the vertical thickness of the upper wall is 215 μm and the lateral wall thickness in the xy plane (t) is 400 μm, which is equal to the outer radius. Afterwards, the internal radius ($\boldsymbol{r_{in}}$) of the sphere starts to increase and it reaches to a value of 310 μm (at z=330 μm). At the same time, the lateral wall thickness decreases to 170 μm. Thus, the coffee stain effect can generate well-organized and robust 3D structures on a superhydrophobic surface.

Influence of surface hydrophobicity and solution concentration on the topography of the 3D coffee stains

Our studies clearly indicate that contact angle (CA) of the substrate is critical for the formation of 2D or 3D coffee stains. To explore the effect of substrate surface, we kept the concentration of silk solution constant at ca. 7-9% by weight and utilized four different substrates poly(methyl methacrylate) (PMMA) (64°), silicon rubber (PDMS) (94°), Teflon tape (PTFE) (123°) and superhydrophobic silicone-urea copolymer (SHPSU) (165°), where WCA are provided in parenthesis. Images provided in Fig. 3a show the droplet structures on initial (top images), mid (middle images) and final (bottom images) stages of the protein solution evaporation on these surfaces. Droplets on PMMA and PDMS surfaces resulted in coffee stains with flat domes, similar to conventional 2D coffee stain. On the other hand, highly hydrophobic PTFE surface resulted in a collapsed dome indicating a transition from 2D to 3D coffee stain. As the substrate surface became superhydrophobic, the protein

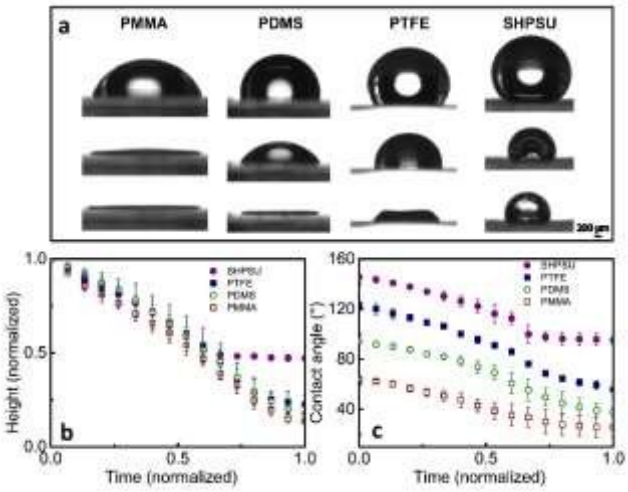

Fig. 3 (a) Images of aqueous silk fibroin droplets on PMMA, PDMS, PTFE and SHPSU at the initial (top images), mid (middle images) and final (bottom images) stages of evaporation, and time dependent **(b)** droplet height, and (**c)** contact angle.

deposition on the pinned base increased leading to skin formation and a stable 3D dome (Fig. 3b). For all samples the droplet heights decreased with time until reaching a stable level. Only the droplet on the superhydrophobic surface exhibited an earlier plateau value for dome height. Moreover, there is a correlation between the initial CA of the solution and final CA of the solid structure. As the hydrophobicity of the surface increases, the final value of the contact angle increases as well (Fig. 3c). While CA of the droplets on all surfaces continue their decrease until complete evaporation, the superhydrophobic surface, which starts with a CA of 145°, reaches to a fairly high final CA of 95°. These results clearly demonstrate the critical effect of surface hydrophobicity on the formation of 3D coffee stain.

Effect of solution concentration on the formation and the structure of the 3D coffee stain was also investigated. For this purpose droplets were deposited on superhydrophobic surface using silk fibroin solutions with concentrations of 1.0, 2.0, 4.0 and 8.0 wt%. As

View Article Online
DOI: 10.1039/C7QM00315F

expected, the initial CA is highest for the solution with lowest concentration, which approaches to the water contact angle (without any protein). On the other hand, the final CA of 3D stains gradually fall, while the concentration decreases because lower concentration leads to a weak skin formation that starts to perturb the spherical shape of the dome and may even collapse (see 1% and 2% solutions in Fig. 4a). As the concentration increases, a self-standing and spherical 3D coffee stain is formed. In addition, the time to reach plateau values decreases with increasing concentration as expected (Fig. 4b and c).

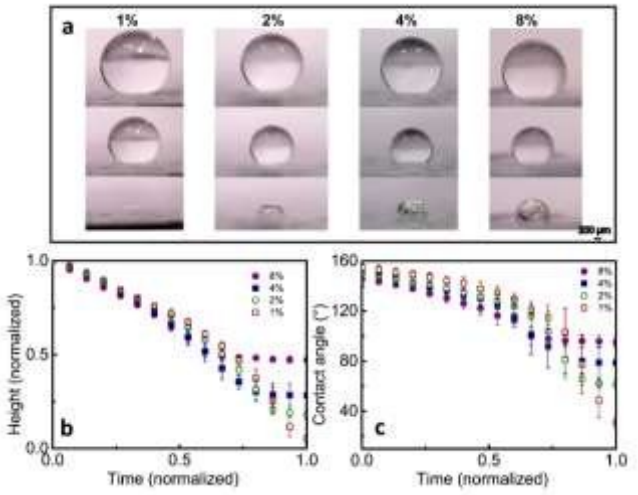

Fig. 4 (a) Images of aqueous silk fibroin droplets with different concentrations on SHPSU surfaces at the initial (top images), mid (middle images) and final (bottom images) stages of evaporation, and time dependent **(b)** droplet height, and **(c)** contact angle.

3D coffee stains for lasers

Spherical 3D coffee stains with a smooth surface can facilitate the light oscillation in solid-air boundary that can generate a whispering gallery mode resonator. Even though the superhydrophobic surfaces were useful to generate 3D stains, the quality of the surfaces obtained were not at a sufficent level to utilize it as an optical cavity. As a further improvement in the structure and the surface quality of 3D coffee stains, we adapted a pendant-drop approach. A blunt stainless steel needle was used to suspend a pendant droplet of aqueous enhanced green fluorescent protein (eGFP) blended silk fibroin solution. The spherical shape of the pendant droplet was maintained throughout the evaporation process due to a very small contact area with the needle tip. Although a perfectly spherical droplet is expected due to minimization of surface energy, as shown in Fig. 5, a slightly elongated pendant droplet is formed as a result of the gravitational force. As shown in the superimposed images provided in Fig. 5a, until the outer skin is formed, the droplet diameter shows a fairly constant rate of decrease with a slope of 0.036 mm^2/s (Fig. 5b), which is almost identical to that of the sessile droplet. As the evaporation proceeds, the skin formed adheres to the tip of the needle and an air bubble is formed similar to those observed on superhydrophobic surfaces. The shape and the size of the droplet does not change after the skin formation and the air bubble keeps expanding until complete evaporation of water, eventually leading to the formation of a spherical 3D coffee stain with enhanced surface quality as shown in Fig. 5c. We also prepared hollow spheres using aquaeous solutions of synthetic polymers, such as polyvinylpyrrolidone and polyvinylalcohol as provided in Fig. S2.

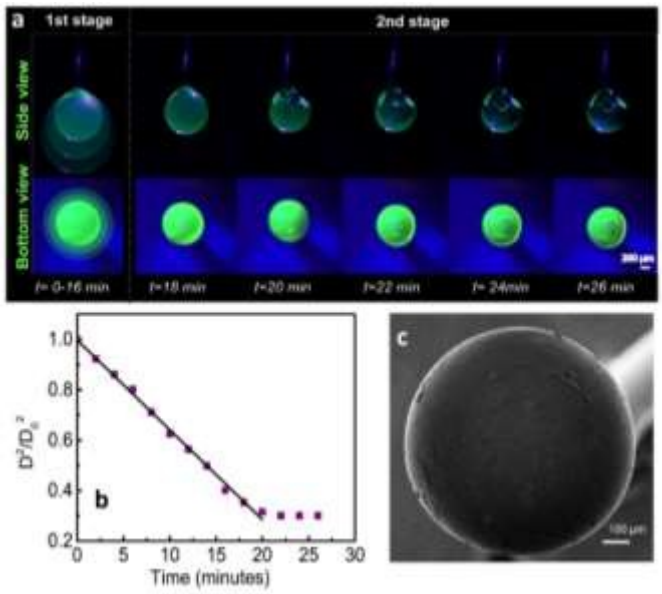

Fig. 5 (a) 3D coffee stain formation from aqueous eGFP modified silk fibroin pendant droplet. **(b)** Change in the pendant droplet diameter (D^2/D_0^2) as a function of time. **(c)** SEM image of 3D coffee stain (bottom view).

To generate an all-protein laser, initially we explored the amplified spontaneous emission (ASE) of eGFP in transparent silk fibroin protein. A thin film of silk fibroin containing eGFP was utilized for ASE experiments via variable stripe length (VSL) method. Using a cylindrical lens, a focused narrow line of laser beam at 482 nm, which overlaps with the strong absorption band of the eGFP, excited a stripe on the slide, which functioned as a one dimensional optical amplifier. While spontaneous emission was generated in random directions as the pump flux was increased, emitted photons were amplified through the stripe due to population inversion and were collected. As shown in Fig. 6a, the spectral narrowing at 521 nm clearly demonstrates the amplified spontaneous emission (Fig. 6b). This result shows that fluorescent protein in a silk fibroin matrix has the potential to generate laser emission in a cavity structure.

Spherical 3D coffee stains obtained by using pendant droplets advantageously increase the surface quality for lasing (Fig. 6c). To generate laser emission, eGFP containing silk fibroin spheroid was pumped with 5 ns OPO pulses ranging from 0.3 µJ to 234.7 µJ at 482 nm and a laser threshold behaviour was observed at 37.15 µJ, where the slope efficiency increased 7.3 times in comparison with subthreshold condition (Fig. 6d and e). Laser emission was further confirmed with spectral narrowing above the threshold. Even though in the subthreshold regime the peak at 521 nm dominates the emission due to amplified spontanous emission, in the suprathreshold region a new and narrowing peak due laser emission is observed at 547 nm, which drastically increases above the threshold (Fig. 6f).

View Article Online
DOI: 10.1039/C7QM00281E

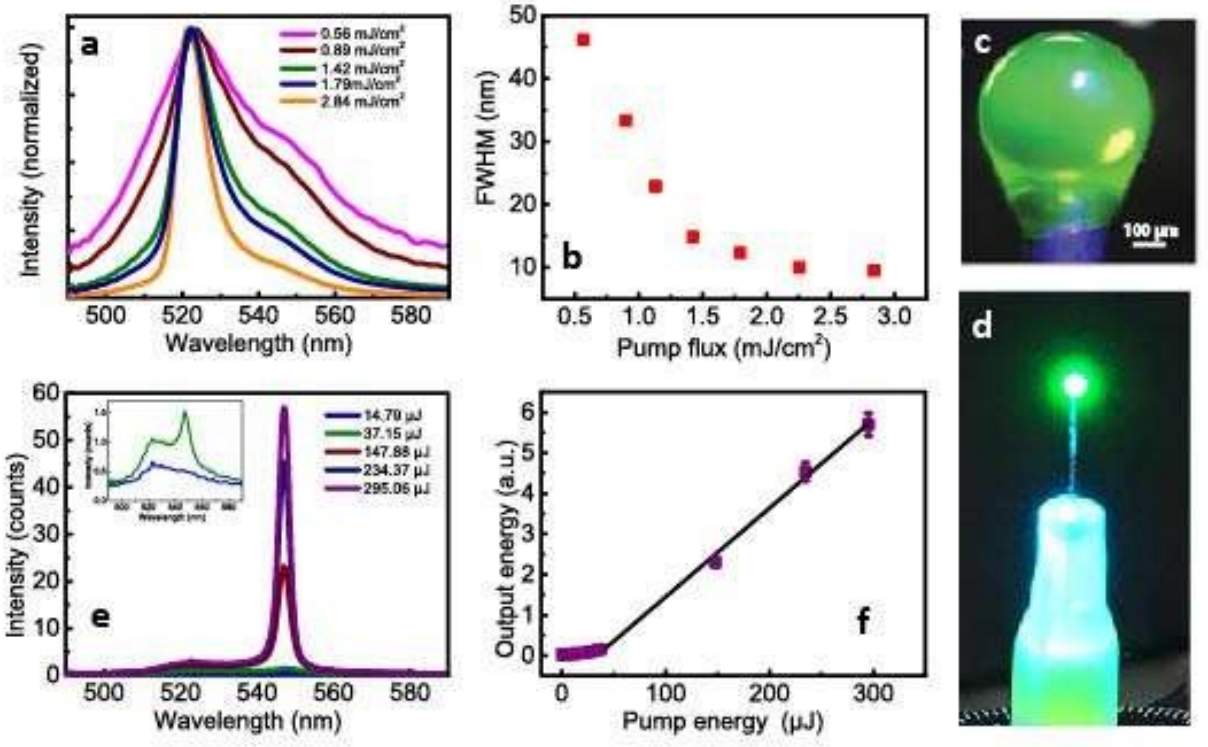

Fig. 6 (a) ASE spectra of spin coated eGFP modified silk fibroin protein film under various pump levels. **(b)** Full width at half maximum (FWHM) of ASE as a function of pump flux. **(c)** The picture of the 3D protein stain under blue light and **(d)** while lasing. **(e)** Emission spectra of protein laser at different pump levels. Inset: Zoomed emission spectrum at 14.79 and 37.15 µJ. **(f)** Output energy of protein laser as a function of pump energy.

Thus, the threshold and spectral behaviour proves the laser emission by the 3D stain. Due to the limited resolution of the detector (≈ 1 nm) the longitudinal and transverse modes were not distinguishable for such a milimeter-scale sphere. The 3D spheres obtained using aqueous silk fibroin solutions, which are biodegradable, biocompatible and transparent have unique properties for cavity formation. Moreover, the biologically produced fluorescent protein of eGFP presents an important natural biomolecule as a laser gain medium in silk fibroin (39). Thus, the spherical 3D coffee stains obtained using pendant droplets of eGFP modified silk fibroin solutions enabled the construction of all-protein lasers.

Conclusions

In conclusion, while hydrophilic surfaces lead to formation of conventional 2D coffee stain, it has been demonstrated that superhydrophobic surfaces facilitate the formation of 3D coffee stain. The 3D coffee stain formation starts with the evaporation of the droplets where the particles move toward the pinned edges and leading to skin formation. As the evaporation continues a bubble nucleates, expands and forms a hollow cavity inside the skin, which results in 3D coffee stain formation. Furthermore, spherical 3D coffee stains with excellent surface quality can be produced by the evaporation of a pendant droplet which leads to all-protein lasers when eGFP doped silk fibroin proteins are utilized. The spheres can further be modified with a wide variety of magnetic and optical nanomaterials to demonstrate novel free-standing devices by self-assembly. Furthermore, this study can open-up new scientific venues on the dynamics and modelling of interfacial interactions and investigations of unconventional 3D systems.

References

1. Eral HB, Augustine DM, Duits MHG, Mugele F. Suppressing the coffee stain effect: how to control colloidal self-assembly in evaporating drops using electrowetting. Soft Matter. 2011;7(10):4954-8.
2. Deegan RD, Bakajin O, Dupont TF, Huber G, Nagel SR, Witten TA. Capillary flow as the cause of ring stains from dried liquid drops. Nature. 1997;389(6653):827-9.
3. Yunker PJ, Durian DJ, Yodh AG. Coffee rings and coffee disks: Physics on the edge. Phys Today. 2013;66(8):60-1.
4. Yunker PJ, Lohr MA, Still T, Borodin A, Durian DJ, Yodh AG. Effects of Particle Shape on Growth Dynamics at Edges of Evaporating Drops of Colloidal Suspensions. Phys Rev Lett. 2013;110(3).
5. Whitesides GM, Boncheva M. Beyond molecules: Self-assembly of mesoscopic and macroscopic components. Proceedings of the National Academy of Sciences. 2002;99(8):4769-74.
6. Whitesides GM, Grzybowski B. Self-assembly at all scales. Science. 2002;295(5564):2418-21.

7. Boal AK, Ilhan F, DeRouchey JE, Thurn-Albrecht T, Russell TP, Rotello VM. Self-assembly of nanoparticles into structured spherical and network aggregates. Nature. 2000;404(6779):746-8.
8. Moreau WM. Semiconductor lithography: principles, practices, and materials: Springer Science & Business Media; 2012.
9. Jackman RJ, Wilbur JL, Whitesides GM. Fabrication of submicrometer features on curved substrates by microcontact printing. Science. 1995;269(5224):664.
10. Lipson H, Kurman M. Fabricated: The new world of 3D printing: John Wiley & Sons; 2013.
11. Bohez EL. Five-axis milling machine tool kinematic chain design and analysis. International Journal of Machine Tools and Manufacture. 2002;42(4):505-20.
12. Misawa H, Juodkazis S. 3D laser microfabrication: principles and applications: John Wiley & Sons; 2006.
13. Mirkin CA, Letsinger RL, Mucic RC, Storhoff JJ. A DNA-based method for rationally assembling nanoparticles into macroscopic materials. Nature. 1996;382(6592):607-9.
14. Mucic RC, Storhoff JJ, Mirkin CA, Letsinger RL. DNA-directed synthesis of binary nanoparticle network materials. Journal of the American Chemical Society. 1998;120(48):12674-5.
15. Alivisatos AP, Johnsson KP, Peng X, Wilson TE, Loweth CJ, Bruchez Jr MP, et al. Organization of'nanocrystal molecules' using DNA. Nature. 1996;382(6592):609-11.
16. Timonen JV, Latikka M, Leibler L, Ras RH, Ikkala O. Switchable static and dynamic self-assembly of magnetic droplets on superhydrophobic surfaces. Science. 2013;341(6143):253-7.
17. Andres RP, Bielfeld JD, Henderson JI, Janes DB. Self-assembly of a two-dimensional superlattice of molecularly linked metal clusters. Science. 1996;273(5282):1690.
18. Van Hameren R, Schön P, Van Buul AM, Hoogboom J, Lazarenko SV, Gerritsen JW, et al. Macroscopic hierarchical surface patterning of porphyrin trimers via self-assembly and dewetting. Science. 2006;314(5804):1433-6.
19. Han W, Lin Z. Learning from "Coffee Rings": Ordered Structures Enabled by Controlled Evaporative Self-Assembly. Angewandte Chemie International Edition. 2012;51(7):1534-46.
20. Yunker PJ, Still T, Lohr MA, Yodh A. Suppression of the coffee-ring effect by shape-dependent capillary interactions. Nature. 2011;476(7360):308-11.
21. Marín ÁG, Gelderblom H, Lohse D, Snoeijer JH. Order-to-disorder transition in ring-shaped colloidal stains. Phys Rev Lett. 2011;107(8):085502.
22. Ma H, Hao J. Ordered patterns and structures via interfacial self-assembly: superlattices, honeycomb structures and coffee rings. Chem Soc Rev. 2011;40(11):5457-71.
23. Shen X, Ho C-M, Wong T-S. Minimal size of coffee ring structure. The Journal of Physical Chemistry B. 2010;114(16):5269-74.
24. Kaplan CN, Wu N, Mandre S, Aizenberg J, Mahadevan L. Dynamics of evaporative colloidal patterning. Phys Fluids. 2015;27(9).
25. Kaplan CN, Mahadevan L. Evaporation-driven ring and film deposition from colloidal droplets. J Fluid Mech. 2015;781.
26. Davidson ZS, Huang Y, Gross A, Martinez A, Still T, Zhou C, et al. Deposition and drying dynamics of liquid crystal droplets. Nature Communications. 2017;8:15642.
27. Sen D, Mazumder S, Melo J, Khan A, Bhattyacharya S, D'souza S. Evaporation driven self-assembly of a colloidal dispersion during spray drying: volume fraction dependent morphological transition. Langmuir. 2009;25(12):6690-5.
28. Crivoi A, Duan F. Three-dimensional Monte Carlo model of the coffee-ring effect in evaporating colloidal droplets. Sci Rep-Uk. 2014;4.
29. Sadek Cl, Tabuteau H, Schuck P, Fallourd Y, Pradeau N, Le Floch-Fouéré Cc, et al. Shape, shell, and vacuole formation during the drying of a single concentrated whey protein droplet. Langmuir. 2013;29(50):15606-13.
30. Pauchard L, Allain C. Stable and unstable surface evolution during the drying of a polymer solution drop. Phys Rev E. 2003;68(5):052801.
31. Marín ÁG, Gelderblom H, Susarrey-Arce A, van Houselt A, Lefferts L, Gardeniers JG, et al. Building microscopic soccer balls with evaporating colloidal fakir drops. Proceedings of the National Academy of Sciences. 2012;109(41):16455-8.
32. Accardo A, Gentile F, Mecarini F, De Angelis F, Burghammer M, Di Fabrizio E, et al. In situ X-ray scattering studies of protein solution droplets drying on micro-and nanopatterned superhydrophobic PMMA surfaces. Langmuir. 2010;26(18):15057-64.
33. Accardo A, Di Stasio F, Burghammer M, Riekel C, Krahne R. Nanocrystal Self-Assembly into Hollow Dome-Shaped Microstructures by Slow Solvent Evaporation on Superhydrophobic Substrates. Particle & Particle Systems Characterization. 2015;32(5):524-8.
34. Parisse F, Allain C. Drying of colloidal suspension droplets: experimental study and profile renormalization. Langmuir. 1997;13(14):3598-602.
35. Zhang Y, Yang S, Chen L, Evans J. Shape changes during the drying of droplets of suspensions. Langmuir. 2008;24(8):3752-8.
36. Söz CK, Yilgör E, Yilgör I. Influence of the coating method on the formation of superhydrophobic silicone–urea surfaces modified with fumed silica nanoparticles. Progress in Organic Coatings. 2015;84:143-52.
37. Chen R-H, Phuoc TX, Martello D. Effects of nanoparticles on nanofluid droplet evaporation. International Journal of Heat and Mass Transfer. 2010;53(19):3677-82.
38. Zhang J, Du S, Kafi A, Fox B, Li JL, Liu XY, et al. Surface energy of silk fibroin and mechanical properties of silk cocoon composites. Rsc Adv. 2015;5(2):1640-7.
39. Gather MC, Yun SH. Bio-optimized energy transfer in densely packed fluorescent protein enables near-maximal luminescence and solid-state lasers. Nature communications. 2014;5:5722.
40. Rockwood DN, Preda RC, Yucel T, Wang XQ, Lovett ML, Kaplan DL. Materials fabrication from Bombyx mori silk fibroin. Nat Protoc. 2011;6(10):1612-31.
41. Söz CK, Yilgör E, Yilgör I. Influence of the average surface roughness on the formation of superhydrophobic polymer surfaces through spin-coating with hydrophobic fumed silica. Polymer. 2015;62:118-28.
42. Söz CK, Yilgör E, Yilgör I. Simple processes for the preparation of superhydrophobic polymer surfaces. Polymer. 2016;99:580-93.

Acknowledgements

S.N. acknowledges the support by Marie Curie Career Integration Grant (PROTEINLED, 631679), and The Scientific and Technological Research Council of Turkey (TUBITAK) under projects 114F317, 115F451. Also, SN acknowledges additional support from the Turkish Academy of Sciences Distinguished Young Scientist Award (TUBA GEBIP) and FABED Eser Tümen Research Award. We thank Prof. Kerem Pekkan and Selda

View Article Online
DOI: 10.1039/C7QM00281E

Göktaş for their support in confocal microscopy measurements and Özgün Can Önder for his assistance of taking SEM images.

Experimental

Materials

Poly(methyl methacrylate) (PMMA) (M_n=190,000, M_w=305,000 g/mol) was synthesized in our laboratories. PDMS was prepared using Sylgard® 184 Silicone Elastomer kit. Teflon tapes were obtained from Resiflon, Du Pont, Italy. Polydimethylsiloxane-urea copolymer (Geniomer TPSC 140) with a PDMS (M_n=3200 g/mol) content of about 92% by weight and hydrophobic fumed silica (HDK H2000) were kindly provided by Wacker Chemie, Munich, Germany. Primary particle size for fumed silica is reported to be 5−30 nm, which increases to 100−250 nm after aggregation. The specific surface area of the particles is 170−230 m^2/g. Deionized and triple distilled water was prepared in our laboratories. Reagent grade solvents, toluene, isopropyl alcohol (IPA) and tetrahydrofuran (THF) were obtained from Merck and used as received.

Preparation of aqueous silk fibroin solution

5 g *Bombyx Mori* silk cocoons were boiled in 2 L of 0.02 M aqueous Na_2CO_3 solution for 30 min to remove sericin and extract the fibroin. Extracted silk fibroin was rinsed and stirred in cold deionized water twice after changing the water between each process and then dried in air at room temperature. Dried silk fibroin was dissolved in 9.3 M LiBr solution and placed in an oven at 60 °C for 4 hours. Viscous silk fibroin solution was injected into a dialysis cassette to separate LiBr and other contaminants. This procedure was continued for 2 days changing the water at time intervals. Finally the silk fibroin solution taken from dialysis cassette was centrifuged at 9000 rpm at -2°C for 20 minutes twice (40). Final concentration of the silk fibroin solution was determined by Gravimetric Analysis and it was measured between 7 and 9 wt%.

Fluorescent Protein expression and purification

GFP fluorescent proteins are prepared using transformed Escherichia coli cells. First GST tag containing vector is transformed into E. coli cells and cells are grown on plates. eGFP protein is 30 kDa and GST tag is linked to N terminal of the protein which is 26 kDa for eGFP-GST vector. Bacterial colony is chosen and induced at large scale broth. Proteins are expressed using 1 mM isopropyl *β*-d-1-thiogalactopyranoside. After protein expression bacteria cells are pelleted with centrifugal force, and cells are lysed with lysozyme and washed with GST Wash Buffer (1X PBS (phosphate-buffered saline), 0.25 M KCl, freshly supplied with 25 µg/mL LPC, 17.4 µg/mL PMSF, and 10 µg/mL Aprotinin). After freezing-thawing and sonicating the cells, protein purification is performed by superflow glutathione agarose beads. Elution buffer (50 mM Tris pH 8.0, 10 mM Glutathione, freshly supplied with 10 mM DTT, 25 µg/mL LPC) is added to the proteins and proteins are eluted with usage of centrifugal filters. Proteins are concentrated using same filters. As eGFP is concentrated 1X PBS (phosphate buffered saline) is passed through the filter until eGFP is concentrated down to 250-300 µL. Then fluorescent proteins are desalted using dialysis membranes.

Fabrication of the substrates

Smooth surfaces based on PMMA and PSU were prepared by spin coating of polymer solutions on glass substrates (41). Teflon tapes were stretched onto glass lams to obtain flat surfaces. Superhydrophobic polydimethylsiloxane-urea (SHPSU) surfaces were prepared by spin coating of silica dispersions in PSU onto glass substrates as reported earlier (36, 41, 42) (Fig. S3).

Characterization techniques

Static water contact angle measurements were performed on a Dataphysics OCA 35 instrument at room temperature (24±2ºC). Dataphysics OCA 35 instrument was equipped with the SCA 20 software which provided the electronic control of the device parameters and the monitoring and measurement of the contact angles. Contact angles reported are average of minimum three measurements. Bottom view images are taken by Olympus CK40 inverted microscope, the samples were enlightened by an additional blue LED where the side views are recorded simultaneously by a CCD camera. The confocal microscopy is done via a Nikon C2si Confocal Microscope with a scanning laser at a wavelength of 488 nm. Surface structures and topographies were determined with a scanning electron microscope (SEM) (ZEISS EVO LS15) at 2 kV. Samples were coated with a 2 – 3 nm gold layer to minimize the charging of the surface. ATR-IR spectra were recorded on a ThermoScientific Smart iTR spectrometer equipped with diamond ATR crystal, with an incident angle of 42˚. 16 scans were taken for each spectrum with a resolution of 4 cm^{-1}.

Silk fibroin and eGFP thin film preparation for ASE experiments

Silk fibroin solution (7-9 wt %) and concentrated eGFP solution (7.96 mg/mL) is mixed with a ratio of 1:1 in volume. 80 µL of this mixture solution is spin coated on a 1 *mm* x 1 *mm* glass substrate for 1 minute at 3000 rpm.

Silk fibroin and eGFP spheroid crystal for lasing experiments

Silk fibroin solution and concentrated eGFP solution is mixed at a ratio of 1:1 by volume. With a headstand 1 mL injector and 32 G stainless steel blunt needle, small droplet is slowly released to the tip of the needle.

Optical set-up for lasing and ASE experiments

Quanta-Ray INDI pulsed Nd:YAG laser with a BasiScan OPO (SpectraPhysics) is used. The pump with a repetition rate of 10 Hz is passed through an OD filter where the laser energy is adjusted. Then, laser arrives on the sample via a 10X microscope objective. The emitted light from the sample is collected by a fiber placed to the side of the sample (i.e., orthogonal to the direction of the pump light) and reached to the spectrometer (Torus Concave Grating Spectrometer, Ocean Optics) as shown in Fig. S4. For ASE experiment, a

View Article Online
DOI: 10.1039/C7QM00281E

cylindrical lens is inserted in the optical set-up instead of the microscope objective.

Droplet size calculations

All the calculations are done by ImageJ software.

Biography

Prof. Sedat Nizamoglu received his Ph.D. in Electrical and Electronics Engineering in 2011 at Bilkent University, Turkey. Immediately after graduation, he continued as a research fellow with a joint affiliation with Harvard Medical School and Wellman Center for Photomedicine, Massachusetts General Hospital in USA. Currently he is a faculty member at Koç University, Turkey. His research focuses on the demonstration of innovative devices and interfaces for the applications to energy, medicine, and environment. He has published more than 40 research papers in prestigious journals including Nature Communication, Nature Photonics, Advanced Materials and Nano Letters. Recently he was recognized by MIT Technology Review as Innovator Under 35 Turkey, he received Outstanding Young Scientist Award by Turkish Academy of Sciences, and he was awarded an ERC (European Research Council) Starting Grant.